Received: 8 April 2022 | Revised: 6 July 2022 | Accepted: 11 July 2022

DOI: 10.1002/psp4.12849

ARTICLE

Cluster Gauss-Newton method analyses of PBPK model parameter combinations of coproporphyrin-I based on OATP1B-mediated rifampicin interaction studies

Takashi Yoshikado[1] | **Yasunori Aoki**[2] | **Tatsuki Mochizuki**[3] | **A. David Rodrigues**[4] | **Koji Chiba**[1] | **Hiroyuki Kusuhara**[3] | **Yuichi Sugiyama**[2]

[1]Laboratory of Clinical Pharmacology, Yokohama University of Pharmacy, Yokohama, Kanagawa, Japan

[2]Laboratory of Quantitative System Pharmacokinetics/Pharmacodynamics, School of Pharmacy, Josai International University, Tokyo, Japan

[3]Laboratory of Molecular Pharmacokinetics, Graduate School of Pharmaceutical Sciences, the University of Tokyo, Tokyo, Japan

[4]Transporter Sciences Group, ADME Sciences, Medicine Design, Pfizer, Groton, Connecticut, USA

Correspondence

Yuichi Sugiyama, Laboratory of Quantitative System Pharmacokinetics/Pharmacodynamics, School of Pharmacy, Josai International University, 2-3-11 Hirakawa-cho, Chiyoda-ku, Tokyo 102-0093, Japan.
Email: y-sugiyama@jiu.ac.jp

Present address

Yasunori Aoki, AstraZeneca, Mölndal, Sweden

Abstract

Coproporphyrin I (CP-I) is an endogenous biomarker supporting the prediction of drug–drug interactions (DDIs) involving hepatic organic anion transporting polypeptide 1B (OATP1B). We previously constructed a physiologically-based pharmacokinetic (PBPK) model for CP-I using clinical DDI data with an OATP1B inhibitor, rifampicin (RIF). In this study, PBPK model parameters for CP-I were estimated using the cluster Gauss–Newton method (CGNM), an algorithm used to find multiple approximate solutions for nonlinear least-squares problems. Eight unknown parameters including the hepatic overall intrinsic clearance ($CL_{int,all}$), the rate of biosynthesis (v_{syn}), and the OATP1B inhibition constant of RIF($K_{i,u,OATP}$) were estimated by fitting to the observed CP-I blood concentrations in two different clinical studies involving changing the RIF dose. Multiple parameter combinations were obtained by CGNM that could well capture the clinical data. Among those, $CL_{int,all}$, $K_{i,u,OATP}$, and v_{syn} were sensitive parameters. The obtained $K_{i,u,OATP}$ for CP-I was 5.0- and 2.8-fold lower than that obtained for statins, confirming our previous findings describing substrate-dependent $K_{i,u,OATP}$ values. In conclusion, CGNM analyses of PBPK model parameter combinations enables estimation of the three essential parameters for CP-I to capture the DDI profiles, even if the other parameters remain unidentified. The CGNM also clarified the importance of appropriate combinations of other unidentified parameters to enable capture of the CP-I concentration time course under the influence of RIF. The described CGNM approach may also support the construction of robust PBPK models for additional transporter biomarkers beyond CP-I.

Study Highlights

WHAT IS THE CURRENT KNOWLEDGE ON THE TOPIC?

Coproporphyrin I (CP-I), an endogenous OATP1B substrate, has been recognized as a potential biomarker for drug–drug interaction (DDI) risk assessment. Strong

OATP1B inhibitors, such as rifampicin (RIF) are known to change the CP-I blood levels.

WHAT QUESTION DID THIS STUDY ADDRESS?

Among many unknown CP-I physiologically-based pharmacokinetic (PBPK) model parameters, how many can be identified by fitting to the clinical data using the cluster Gauss–Newton method (CGNM)? Can even the unidentified parameters be used for predicting other drug interactions?

WHAT DOES THIS STUDY ADD TO OUR KNOWLEDGE?

CGNM estimated eight PBPK model parameters. However, three key parameters were identifiable (hepatic overall intrinsic clearance, CP-I biosynthesis rate, and OATP1B K_i for RIF). The appropriate combinations of an additional five unidentifiable parameters were also deemed important in order to capture the time profiles of CP-I.

HOW MIGHT THIS CHANGE DRUG DISCOVERY, DEVELOPMENT, AND/OR THERAPEUTICS?

Our methodology can enable the construction of robust PBPK model for new DDI transporter biomarkers, even if there is difficulty in estimating all the model parameters.

INTRODUCTION

Modeling-based prediction of drug–drug interactions (DDIs) has become standard practice in various stages of drug research and development. Several drug-metabolizing enzymes and transporters have been identified as key drivers of clinically relevant pharmacokinetic DDIs, which has necessitated the characterization of victim drug pharmacokinetic, efficacy, and safety profile changes. In this regard, the inhibition of hepatic organic anion transporting polypeptides 1Bs (OATP1B1 and OATP1B3), which are multispecific transporters mediating the sinusoidal uptake of various drugs, is one of the important DDI mechanisms. The combinatorial use of OATP1B inhibitors, such as rifampicin (RIF) and cyclosporin A causes a significant increase in the systemic exposure of OATP1B substrates.[1–4] Not surprisingly, regulatory agencies now mandate the reporting of in vitro transporter inhibition data for new chemical entities (NCEs). Upon application of decision trees described in agency guideline documentation, in vitro OATP1B inhibition data for most NCEs can be applied to support DDI risk assessment. However, such approaches may yield relatively high false-positive rates. Even for true-positive rates, it is difficult to predict the magnitude of the potential DDIs.[5]

Various endogenous OATP1B substrates have been proposed as surrogate probes[5–7] to facilitate the risk assessment of pharmacokinetic DDIs in early clinical phases. Among them, the heme synthesis by-product, coproporphyrin I (CP-I),[8–10] has been used as biomarkers for assessing OATP1B-mediated DDIs.[11–18] CP-I has advantages in the evaluation of OATP1B-mediated DDIs, such as negligible effects of food and no circadian rhythm,[9,10] as well as its specificity and sensitivity for OATP1B inhibition. Consequently, the pharmaceutical industry is beginning to use CP-I in combination with other OATP1B-DDI biomarkers in setting exclusion criteria for drug candidates with high DDI risk, guiding decisions regarding the conduct of clinical DDI studies, and designing phase III trials with a minimum risk of DDI.[19]

Modeling and simulation approaches to describe blood concentration–time profiles of CP-I in the absence and presence of OATP inhibitors have been reported using empirical compartment models[20,21] and physiologically-based pharmacokinetic (PBPK) models.[22,23] In our previous study, three unknown PBPK parameters including the hepatic overall intrinsic clearance ($CL_{int,all}$), the biosynthesis rate of CP-I (v_{syn}), and the hepatic OATP1B RIF inhibition constant ($K_{i,u,OATP}$) were estimated using a conventional fitting approach and a nonlinear least-squares algorithm.[22] Starting from one initial parameter combination, only one estimated parameter combination could be obtained. Although such an approach should require expert setting of an adequate initial value for each parameter, it is possible that such a modeling exercise may find a parameter combination at the local minimum by chance. Therefore, it is important to ensure the accuracy and robustness of the parameter values in any PBPK model for CP-I. This can only be investigated by comprehensive analysis of the dependence of initial values and fixed values.

A parameter estimation method called the cluster Gauss–Newton method (CGNM)[24] has emerged. The

CGNM is a numerical algorithm designed to solve nonlinear least squares problem by minimizing the sum of squared residuals (SSRs) defined by Equation 1[24]:

$$\mathrm{SSR} = \sum_{i=1}^{n} \left(\log_{10}\left(y_{\mathrm{obs},i}\right) - \log_{10}\left(y_{\mathrm{pred},i}\right)\right)^2 \quad (1)$$

where $y_{\mathrm{obs},i}$ and $y_{\mathrm{pred},i}$ are the ith observed value and predicted value, respectively. The CGNM can find multiple parameter combinations that minimize the SSR. In our case, the residual is the difference between the observed and model simulated value. CGNM initiates the parameter search from multiple initial estimates and obtains multiple parameter combinations with similarly small SSRs in a computationally efficient manner. The essential difference between CGNM and more conventional parameter estimation methods (e.g., Gauss–Newton method) is that the former does not assume the existence of unique best fit parameter combination that minimizes SSR. The CGNM algorithm tolerates non-identifiable parameters in the analysis and is capable of automatically obtaining multiple parameter combinations while visualizing the identifiability of such parameters by showing the distribution of parameter values and combinations thereof that provide equally good model fits as "the best fit." Therefore, CGNM can support more robust and comprehensive analysis of clinical DDI data while circumventing laborious and time-consuming processes of making the PBPK model identifiable by fixing parameters based on educated guesses relying on the modelers' experience.

In the present study, we analyzed two different clinical CP-I studies, a 2-Dose-RIF study[10] and a second published 3-Dose-RIF study,[7] using CGNM. Six PBPK model parameters for CP-I ($\mathrm{CL}_{\mathrm{int,all}}$, v_{syn}, β, $F_{\mathrm{a}}F_{\mathrm{g}}$, f_{bile}, and f_{syn}), and RIF $K_{i,\mathrm{u,OATP}}$ and $K_{i,\mathrm{u,MRP2}}$ were estimated simultaneously to find identifiable parameters and determine their reproducibility across the two independent studies.

METHODS

Overview of PBPK modeling

The PBPK model structures (Figure S1) for CP-I,[22] RIF,[25] pitavastatin (PTV),[26] and rosuvastatin (RSV)[27] were basically from previously published studies. Our approach of PBPK modeling including modified points for these PBPK models are described in detail in the Supplementary Text. Differential equations and other equation settings describing these PBPK models are also presented in the Supplementary Text. Physiological and pharmacokinetic parameters used in the PBPK models are shown in Table S1A.

Algorithm and software for parameter estimation

The parameter estimation for the PBPK models of CP-I, RIF, PTV, and RSV was performed using the GUI software of CGNM, version a6.2.2 (http://www.bluetree.me/CGNmethod_for_PBPKmodels). The CGNM algorithm finds multiple parameter combinations that minimize the SSR.[24] Given there was a reported inhibition constant of hepatic MRP2 ($K_{i,\mathrm{u,MRP2}}$) value from the in vivo experiment, we also included this value as an observation for the parameter estimation of CP-I. In other words, we found parameter combinations that minimize the following:

$$\mathrm{SSR}' = \sum_{i=1}^{n} \left(\log_{10}\left(y_{\mathrm{obs},i}\right) - \log_{10}\left(y_{\mathrm{pred},i}\right)\right)^2 + \mathrm{weight} \times \left(\log_{10}\left(\text{estimated } K_{i,\mathrm{u,MRP2}}\right) - \log_{10}\left(\text{reported in vivo } K_{i,\mathrm{u,MRP2}}\right)\right)^2, \quad (2)$$

where the weight is an arbitrary chosen constant, and the reported in vivo $K_{i,\mathrm{u,MRP2}}$ (0.87 μM)[22] was estimated based on the change in the biliary clearance of [^{11}C]-TIC-Me, a positron emission tomography (PET) probe for OATP1B and MRP2.[28] Because the sum of two quantities that are fundamentally different was minimized, we tested the optimization with various weights and chose 0.1 so that the estimated $K_{i,\mathrm{u,MRP2}}$ varied more than 10-fold between the minimum and the maximum values.

In simple terms, CGNM finds multiple sets of parameters that fit the observation by conducting the Gauss–Newton optimization from various initial iterates in a computationally efficient manner. The initial iterates are created randomly based on the user-defined initial lower and upper ranges for each unknown parameter. The initial lower and upper ranges were set to the base values (the reported values in the literature) multiplied by 10^{-2} and 10^{2}, respectively (Table S1B–E). For the unknown parameters describing a kind of fraction, the initial lower and upper ranges were set at 0.01 and 0.99, respectively. Within the initial range, 1000 parameter combinations were generated as initial clusters that were then improved by 50 iterations.

Application of the CGNM to PBPK modeling and simulation

The flowchart for the PBPK-CGNM analyses is shown in Figure S2a. After running the CGNM, parameter combinations that could well explain the blood concentration data were selected by the cutoff method composed of two steps[29]: [i] Chi-square method, which rejects parameter combinations with significantly larger SSRs than the minimum SSR by assuming a Chi-square distribution of SSR (alpha value = 0.05), and [ii] the Elbow method,

which chooses the cutoff so that the sum of the areas of two trapezoids in the order SSR plot among the SSRs that are not rejected by [i] becomes a minimum (Figure S2b). Although it is assumed that multiple parameter combinations exist with exactly the same minimum SSR, such multiple parameter combinations were not found due to an artifact of numerical computation. Therefore, parameter combinations with SSRs that were "quite similar" were determined by the two-step cutoff method. To show the distribution of estimated parameters, namely the median, 25th, and 75th percentiles, and minimum and maximum values, violin plots composed of a box plot and a kernel density plot were used. The variability of parameters obtained by our CGNM analyses could be ascribed to the fact that each parameter is not uniquely determined. Hence, the variability of the DDI simulation does not include interindividual variability.

An example of R script for the CGNM analysis (CP-I vs. 3-Dose-RIF) is attached as a Supplementary Model File.

Model predictability

To evaluate model predictability, the average fold errors (AFEs) for area under the blood concentration–time curve (AUC), maximum blood concentration (C_{max}), and their ratios were calculated as shown in Equation 3:

$$\mathrm{AFE} = 10^{\frac{\sum_{i=1}^{n}\left|\log\frac{\text{Simulated}}{\text{Observed}}\right|}{n}}, \quad (3)$$

where n is the number of observations.

RESULTS

CGNM analyses for RIF in the 2-Dose-RIF and 3-Dose-RIF studies

Although the PBPK model and parameters for RIF reported previously[25] could almost explain the blood concentration–time profiles in the 2-Dose-RIF study,[10] the model and parameters underestimated the observed blood concentrations in the 3-Dose-RIF study.[7] To explain the blood concentration–time profiles of RIF from the two clinical studies[7,10] comprehensively, we modified the PBPK model, as described in the Methods section. We first estimated eight unknown parameters ($CL_{int,all}$, f_{bile}, $K_{m,u,OATP}$, k_a, $K_{p,Scale}$, k_{sto}, $PS_{dif,ent}$, and R_{dif}, as shown in Table S2) using the data from the 3-Dose-RIF study. Subsequently, three parameters ($K_{m,u,OATP}$, $K_{p,Scale}$, and R_{dif}) were fixed and the other five parameters were estimated for the 2-Dose-RIF study. After optimization by CGNM, 915 and 795 parameter combinations were selected by the two-step cutoff (Chi-square and Elbow methods) for the 2-Dose-RIF and 3-Dose-RIF studies (Figure S3a and d), respectively, which explained the observed blood concentrations of RIF comprehensively (Figure S3b and e). Distribution of the estimated parameters is shown in Figure S3c and f as violin plots. Statistics for the estimated parameters are summarized in Table S2.

CGNM analyses for CP-I in the 2-Dose-RIF study

After generating 1000 initial parameter combinations for eight unknown parameters, parameter estimation by CGNM was performed using the 2-Dose-RIF study data.[10] As a result, 521 parameter combinations were selected (Figure 1a) that could explain the observed blood concentrations of CP-I in the absence and presence of RIF at 300 and 600 mg orally (Figure 1b). Distribution of the directly estimated parameters is shown in Figure 1c. Statistics for the estimated parameters (median, 25th, and 75th percentiles, and minimum and maximum values) are summarized in Table 1. $CL_{int,all}$, $K_{i,u,OATP}$, and v_{syn} were obtained within relatively narrow ranges. The medians for $K_{i,u,OATP}$, $CL_{int,all}$, and v_{syn} were 0.048 μM (quartile, 0.044–0.055 μM), 44 L/h/kg (quartile, 41–48 L/h/kg), and 0.22 nmol/h/kg (quartile, 0.20–0.25 nmol/h/kg), respectively. The other estimated parameters (β, F_aF_g, f_{bile}, $K_{i,u,MRP2}$, and f_{syn}) were obtained with broad ranges of distribution. By parameter transformation from the hybrid parameters to the hepatic intrinsic clearances for primary processes, $CL_{int,bile}$, $CL_{int,met}$, $PS_{act,inf}$, $PS_{dif,inf}$, and PS_{eff} were obtained with broad ranges (Figure 1d and Table 1).

CGNM analyses were also performed to reproduce the results obtained by the previous PBPK analyses using the conventional nonlinear least-squares method.[22] The PBPK model structure and parameters of RIF used in these analyses were exactly the same as those used in the previous study. For CP-I, by fixing four parameters (β = 0.5, f_{bile} = 0.84, $K_{i,u,MRP2}$ = 0.87 μM, and f_{syn} = 1) at the exact values fixed in the previous study, the other four parameters (F_aF_g, $CL_{int,all}$, $K_{i,u,OATP}$, and v_{syn}) were estimated by CGNM (Figure S4). The blood concentration–time profiles in the 2-Dose-RIF study[10] were almost exactly reproduced by these settings of the model and parameters. The obtained parameters were ca. 41 L/h/kg, 0.40, 0.085 μM, and 0.24 nmol/h/kg for $CL_{int,all}$, F_aF_g, $K_{i,u,OATP}$, and v_{syn}, respectively (Table S3), and are similar to those obtained in the previous study (38 L/h/kg, 0.31, 0.097 μM, and 0.26 nmol/h/kg, respectively[22]).

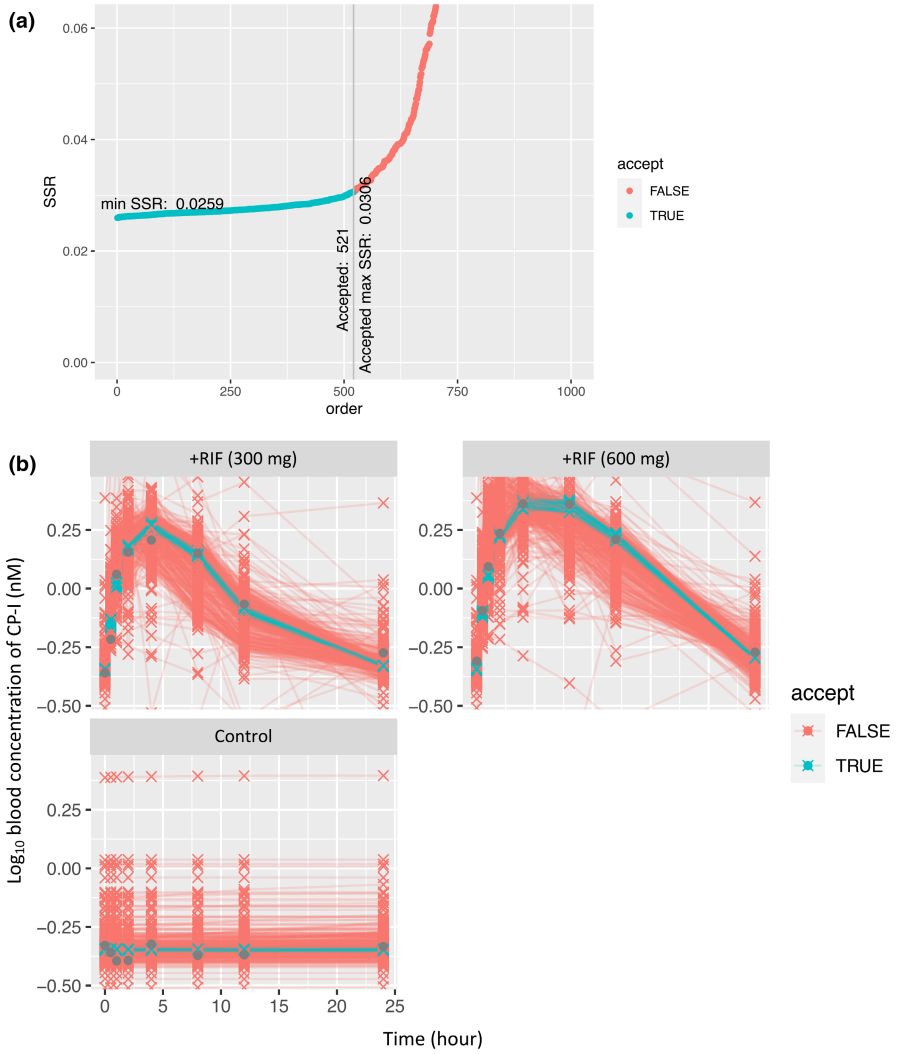

FIGURE 1 Parameter estimation by CGNM using the blood concentration–time profiles of CP-I in the 2-Dose-RIF study. (a) The SSR values for 1000 parameter combinations estimated by CGNM analyses are plotted in ascending order. Green dots indicate SSR values less than 0.0306 (from ranks 1 to 521) selected by the cutoff criteria (Chi-square + Elbow methods); red dots indicate SSR values more than the cutoff criteria. The minimum SSR (rank 1) was 0.0259. (b) The blood concentration–time profiles of CP-I in the absence and presence of RIF were simulated using the parameter combinations obtained by CGNM analyses. Green crosses indicate the time points simulated using the parameter combinations selected by the cutoff criteria (Chi-square + Elbow methods); red crosses indicate those simulated using the nonselected parameter combinations. Gray symbols indicate the clinical data observed in the 2-Dose-RIF study.[10] (c) Violin plots for the directly estimated parameters (β, $CL_{int,all}$, F_aF_g, f_{bile}, $K_{i,u,MRP2}$, $K_{i,u,OATP}$, f_{syn}, and v_{syn}). Note that the in vivo value for $K_{i,u,MRP2}$ (870 nM) estimated based on the change in the biliary clearance of a PET probe (as described in Methods) was included as an observation in the CGNM analysis. (d) Violin plots for the transformed parameters ($CL_{int,bile}$, $CL_{int,met}$, $PS_{act,inf}$, $PS_{dif,inf}$, and PS_{eff}). In each plot, a gray area indicates the distribution of the parameter values, a black dot on the violin plot indicates the median, a black bar in the center of the violin indicates interquartile range, solid lines stretched from the bar indicate the 25th percentile and 75th percentile values, and broken lines indicate the lower/upper adjacent values. CGNM, cluster Gauss–Newton method; CL, clearance; CP-I, coproporphyrin I; PET, positron emission tomography; RIF, rifampicin; SSR, sum of squared residual.

CGNM analyses for CP-I in the 3-Dose-RIF study

We performed the estimation of parameters including $K_{i,u,OATP}$ by CGNM using the remaining clinical data (3-Dose-RIF study[7]). Using eight unknown parameters, including hepatic hybrid parameters, 621 parameter combinations were ultimately selected by the cutoff method (Figure 2a) that could explain the observed blood concentration–time profiles of CP-I in the absence and presence of RIF at 150–600 mg orally (Figure 2b). Distribution of the directly estimated parameters is shown in Figure 2c; statistics for the estimated parameters are summarized in Table 1. Similar to the analyses of the 2-Dose-RIF study, $CL_{int,all}$, $K_{i,u,OATP}$, and v_{syn} were obtained within relatively narrow ranges. The median for

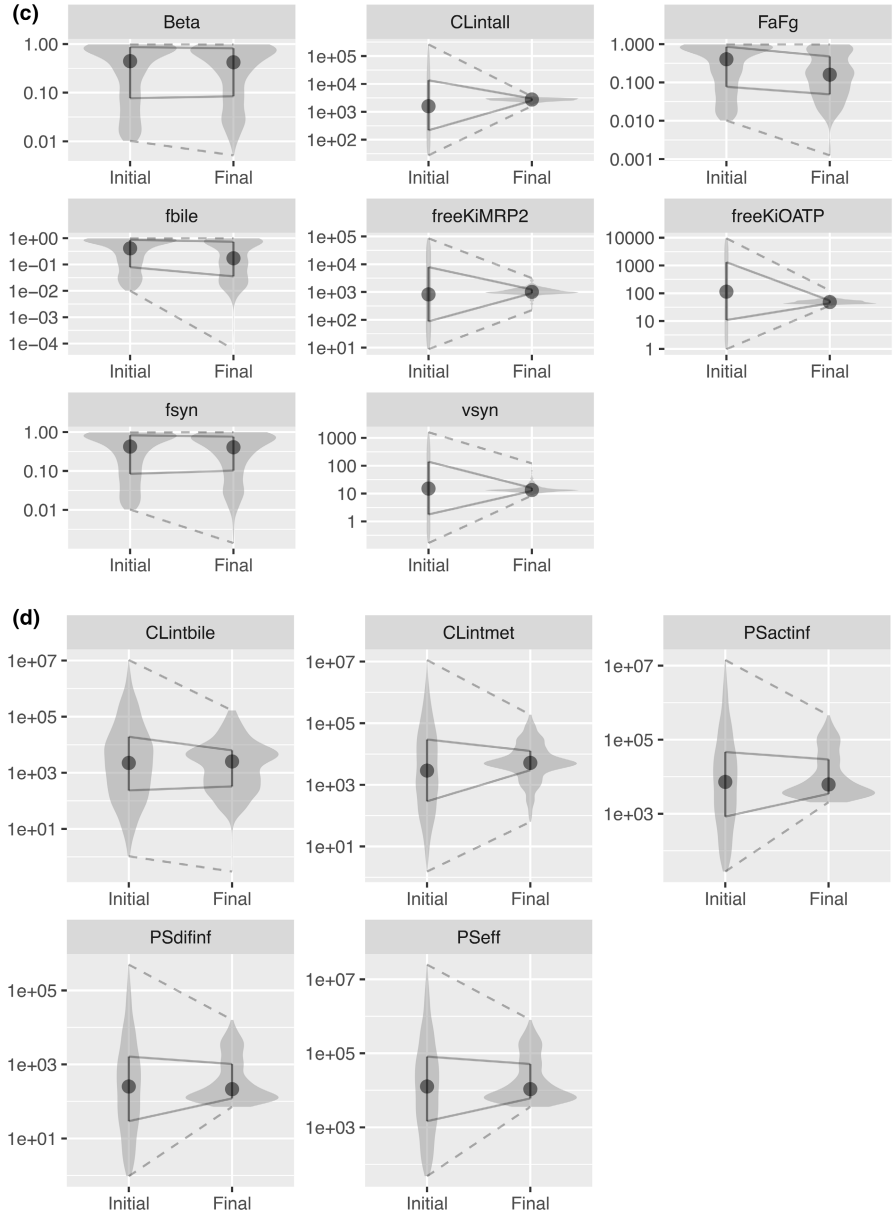

FIGURE 1 (Continued)

$K_{i,u,OATP}$ was 0.053 μM (quartile, 0.046–0.060 μM), which was similar to the value obtained in the analyses of the 2-Dose-RIF study (Table 1). The medians for $CL_{int,all}$ and v_{syn} were 38 L/h/kg (quartile, 35–43 L/h/kg) and 0.19 nmol/h/kg (quartile, 0.17–0.22 nmol/h/kg), respectively. Similar to the results of the 2-Dose-RIF study, the other directly estimated parameters (β, F_aF_g, f_{bile}, $K_{i,u,MRP2}$, and f_{syn}) and transformed parameters ($CL_{int,bile}$, $CL_{int,met}$, $PS_{act,inf}$, $PS_{dif,inf}$, and PS_{eff}) were obtained with broad ranges (Figure 2c,d, and Table 1).

We also applied the CGNM to the individual data from the 3-Dose-RIF study as described in the Supplementary Text. Although some interindividual variabilities of $CL_{int,all}$, $K_{i,u,OATP}$, and v_{syn} were suggested from the results, we obtained essentially similar results to those based on the mean data.

CGNM analyses for statins in the 3-Dose-RIF study

Estimation of parameters, including RIF $K_{i,u,OATP}$ by CGNM, was also performed for statins using the data from the 3-Dose-RIF study.[7] Setting seven and six unknown parameters for PTV and RSV, respectively, 724 and 573 parameter combinations were finally selected (Figures 3a and 4a), which could explain their observed blood concentration–time profiles in the absence and presence of RIF (Figures 3b and 4b). Distributions of the estimated parameters are shown in Figures 3c,d and 4c,d). Statistics for the estimated parameters are summarized in Table 2. The directly estimated parameters for PTV and RSV, except β for PTV, were obtained within narrow ranges. The

TABLE 1 Parameters estimated by the CGNM analyses using the blood concentration-time profiles of CP-I in the 2-Dose-RIF (no. 1) and 3-Dose-RIF (no. 2) studies

Parameter	Unit	Clinical study No.	Minimum	25th percentile	Median	75th percentile	Maximum
β	-	1	0.00515	0.0842	0.421	0.815	0.980
		2	0.00551	0.114	0.499	0.821	0.993
$CL_{int,all}$	L/h/kg	1	25.9	40.5	44.4	48.2	57.6
		2	22.8	34.6	38.3	42.8	47.0
F_aF_g	-	1	0.00126	0.0489	0.160	0.477	0.980
		2	0.00744	0.116	0.260	0.544	0.985
f_{bile}	-	1	0.0000611	0.0354	0.173	0.731	0.986
		2	0.00976	0.106	0.409	0.825	0.998
$K_{i,u,MRP2}$[a]	nmol/L	1	222	908	1010	1.24E+03	3.16E+03
		2	143	831	889	967	4.55E+03
$K_{i,u,OATP}$	nmol/L	1	36.1	43.6	48.4	54.7	127
		2	38.0	45.5	52.6	60.3	575
f_{syn}	-	1	0.00140	0.102	0.407	0.764	0.992
		2	0.00166	0.0733	0.423	0.797	0.991
v_{syn}	nmol/h/kg	1	0.136	0.199	0.215	0.254	1.96
		2	0.108	0.174	0.192	0.224	4.57
$PS_{act,inf}$[b]	L/h/kg	1	32.8	55.5	98.8	472	7.38E+03
		2	26.6	44.8	71.7	313	5.93E+03
$PS_{dif,inf}$[c]	L/h/kg	1	1.15	1.94	3.46	16.5	258
		2	0.978	1.65	2.63	11.5	218
PS_{eff}[d]	L/h/kg	1	57.5	97.1	173	825	1.29E+04
		2	48.9	82.3	132	575	1.09E+04
$CL_{int,bile}$[e]	L/h/kg	1	0.00482	5.25	40.7	101	2.68E+03
		2	0.959	20.3	56.4	131	2.36E+03
$CL_{int,met}$[f]	L/h/kg	1	1.01	48.1	82.9	202	3.04E+03
		2	0.781	20.1	59.9	204	1.01E+04

Note: $CL_{int,all} = (PS_{act,inf} + PS_{dif,inf}) * \beta$; $\beta = (CL_{int,bile} + CL_{int,met})/(PS_{eff} + CL_{int,bile} + CL_{int,met})$; $R_{dif} = PS_{dif,inf}/PS_{act,inf}$; $\gamma = PS_{dif,inf}/PS_{eff}$; $f_{bile} = CL_{int,bile}/(CL_{int,bile} + CL_{int,met})$.[26]

Abbreviations: CGNM, cluster Gauss–Newton method; CP-I, coproporphyrin I; PET, positron emission tomography; RIF, rifampicin.

[a]The in vivo value for $K_{i,u,MRP2}$ (870 nM) estimated based on the change in the biliary clearance of a PET probe (as described in the Methods section) was included as an observation in the CGNM analyses.

[b–f]Hepatic intrinsic clearances for membrane permeation and metabolism processes were transformed from the estimated hybrid parameters ($CL_{int,all}$, β, and f_{bile}) and the fixed hybrid parameters ($R_{dif} = 0.035$ and $\gamma = 0.02$, as described in Table S1) using the equations as follows:

[b]$PS_{act,inf} = 1/(1 + R_{dif}) * CL_{int,all}/\beta$.

[c]$PS_{dif,inf} = R_{dif}/(1 + R_{dif}) * CL_{int,all}/\beta$.

[d]$PS_{eff} = R_{dif}/(1 + R_{dif})/\gamma * CL_{int,all}/\beta$.

[e]$CL_{int,bile} = CL_{int,all}/(1 - \beta) * R_{dif}/(1 + R_{dif})/\gamma * f_{bile}$.

[f]$CL_{int,met} = CL_{int,all}/(1 - \beta) * R_{dif}/(1 + R_{dif})/\gamma * (1 - f_{bile})$.

These equations are derived from those reported for calculating the hybrid parameters.[26]

median for $K_{i,u,OATP}$ by RIF was 0.26 μM (quartile, 0.25–0.27 μM) and 0.15 μM (quartile, 0.14–0.15 μM) for PTV and RSV, respectively.

We also confirmed the applicability of CGNM analyses to the blood concentration–time profiles of PTV and RSV in the 2-Dose-RIF study, as shown in the figures in the Supplementary Text.

Comparison of the simulated and observed AUC and C_{max} and their ratios under DDIs

The simulated AUC and C_{max} of CP-I, PTV, and RSV in the 3-Dose-RIF study using all the estimated parameter combinations including $K_{i,u,OATP}$, selected by the cutoff method in each CGNM analysis, were compared

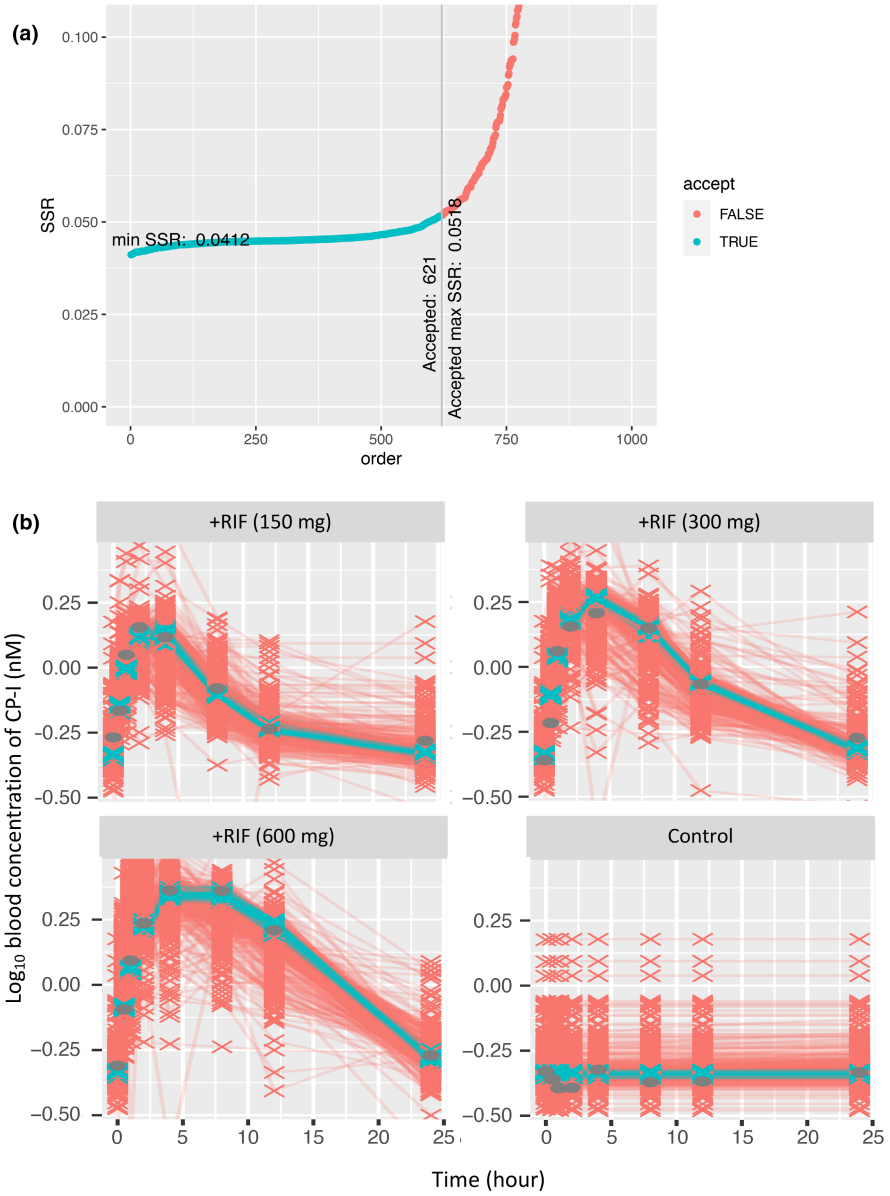

FIGURE 2 Parameter estimation by CGNM using the blood concentration–time profiles of CP-I in the 3-Dose-RIF study. (a) The SSR values for 1000 parameter combinations estimated by CGNM analyses are plotted in ascending order. Green dots indicate SSR values less than 0.0518 (from ranks 1 to 621) selected by the cutoff criteria (Chi-square + Elbow methods); red dots indicate SSR values more than the cutoff criteria. The minimum SSR (rank 1) was 0.0412. (b) The blood concentration–time profiles of CP-I in the absence and presence of RIF were simulated using the parameter combinations obtained by CGNM analyses. Green crosses indicate the timepoints simulated using the parameter combinations selected by the cutoff criteria (Chi-square + Elbow methods); red crosses indicate those simulated using the nonselected parameter combinations. Gray symbols indicate the clinical data observed in the 3-Dose-RIF study.[7] (c) Violin plots for the directly estimated parameters (β, $CL_{int,all}$, F_aF_g, f_{bile}, $K_{i,u,MRP2}$, $K_{i,u,OATP}$, f_{syn}, and ν_{syn}). Note that the in vivo value for $K_{i,u,MRP2}$ (870 nM) estimated based on the change in the biliary clearance of a PET probe (as described in the Methods section) was included as an observation in the CGNM analysis. (d) Violin plots for the transformed parameters ($CL_{int,bile}$, $CL_{int,met}$, $PS_{act,inf}$, $PS_{dif,inf}$, and PS_{eff}). In each plot, a gray area indicates the distribution of the parameter values, a black dot on the violin plot indicates the median, a black bar in the center of the violin indicates interquartile range, solid lines stretched from the bar indicate the 25th percentile and 75th percentile values, and broken lines indicate the lower/upper adjacent values. CGNM, cluster Gauss–Newton method; CL, clearance; CP-I, coproporphyrin I; PET, positron emission tomography; RIF, rifampicin; SSR, sum of squared residual.

with the observed values (Figure 5a,b). AFEs for the AUC and C_{max} were 1.38 and 1.37, respectively. Next, the simulated increased ratios for AUC and C_{max} (AUCR and C_{max}R, respectively) were also plotted against the observed values. AFEs for the AUCR and C_{max}R were 1.17 and 1.34, respectively, using all the estimated parameter combinations including $K_{i,u,OATP}$ (Figure 5c,d).

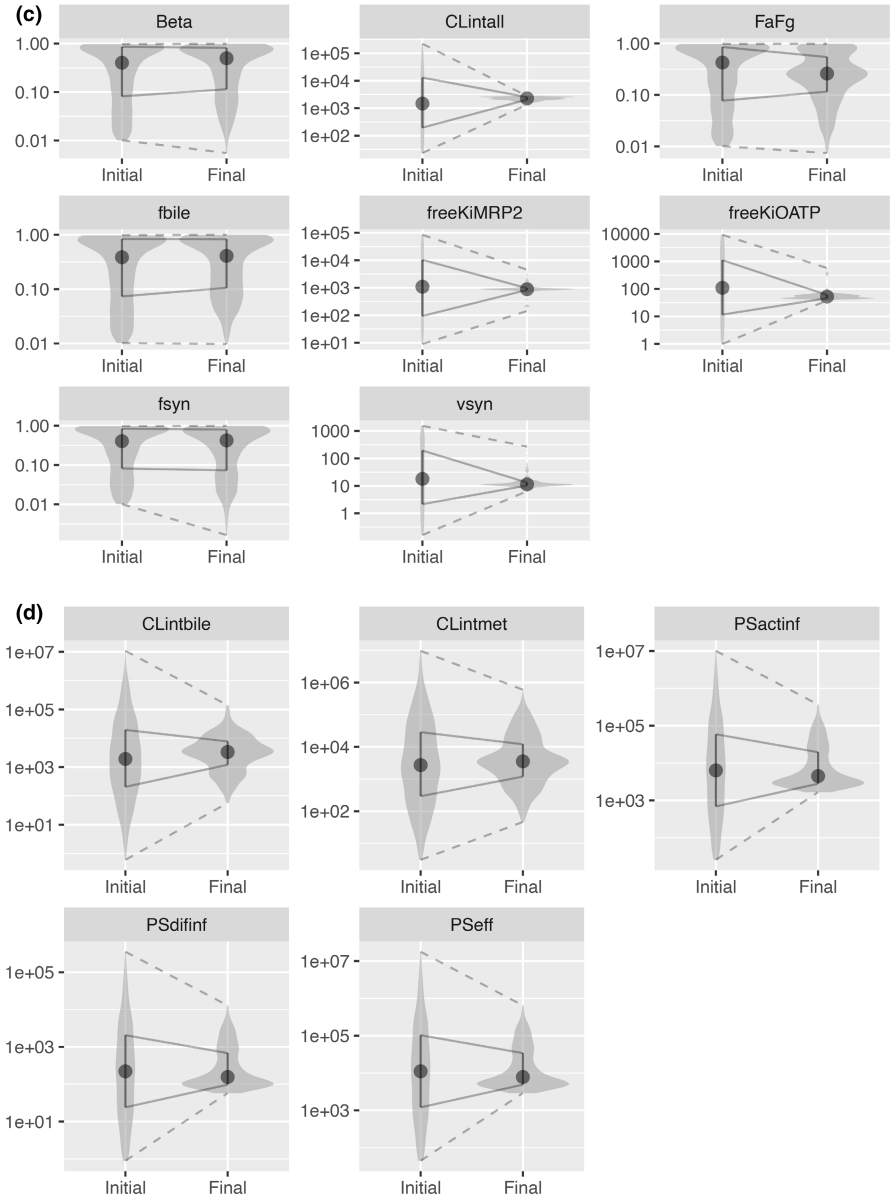

FIGURE 2 (Continued)

DISCUSSION

In the present study, a parameter estimation methodology called CGNM was applied to the PBPK model analyses describing the interaction between CP-I and RIF by leveraging two independent clinical studies to support the reproducibility of the essential parameter estimates across the studies. After generating 1000 initial parameter combinations, 521 and 621 parameter combinations satisfied the acceptance criteria in reproducing the CP-I blood concentration–time profiles in the 2-Dose-RIF and 3-Dose-RIF studies, respectively (Figures 1a,b and 2a,b). Focusing on the violin plot distribution of the estimates, three parameters out of eight, $CL_{int,all}$, v_{syn}, and $K_{i,u,OATP}$, were characterized as relatively sensitive for both studies (Figures 1c and 2c), which was also supported by the calculation of coefficients of variation for these parameters, as shown in the Supplementary Text. Notably, these obtained parameters were similar among the present study, our previous study (conventional method[22]) and the study by Takita et al.[23] as summarized in a table in the Supplementary Text.

In the PBPK model analysis, the validity of the values of model parameters has been carefully surveyed, and there are instances when it is evident that the parameters need to be fixed. Indeed, we introduced three different β values in our previous analysis to avoid divergence and consequently found that β values did not greatly influence the $K_{i,u,OATP}$ value.[22] CGNM analyses in the present study more comprehensively supported the fact that the effect of fixed parameters in the previous analysis on the $K_{i,u,OATP}$ value was minimal, and that the clinical data subjected to

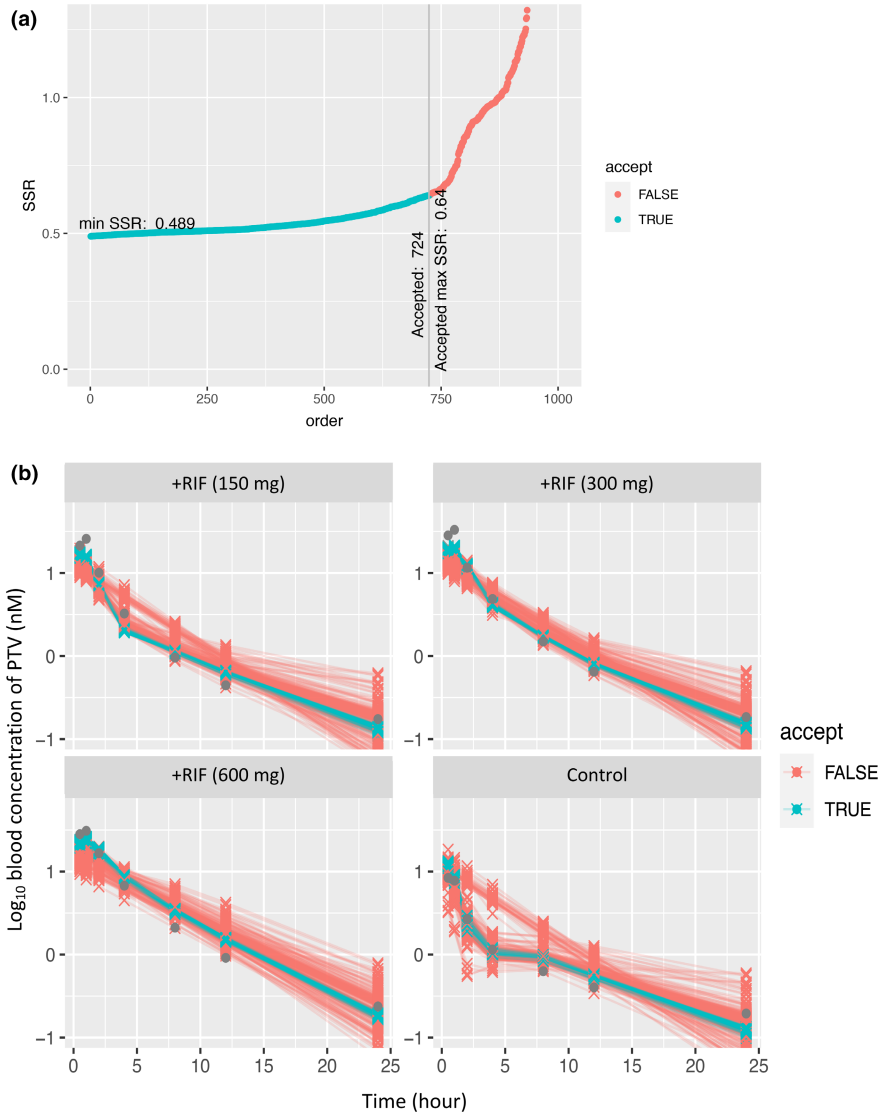

FIGURE 3 Parameter estimation by CGNM using the blood concentration–time profiles of PTV in the 3-Dose-RIF study. (a) The SSR values for 1000 parameter combinations estimated by CGNM analyses are plotted in ascending order. Green dots indicate SSR values less than 0.640 (from ranks 1 to 724) selected by the cutoff criteria (Chi-square + Elbow methods); red dots indicate SSR values more than the cutoff criteria. The minimum SSR (rank 1) was 0.489. (b) The blood concentration–time profiles of PTV in the absence and presence of RIF were simulated using the parameter combinations obtained by CGNM analyses. Green crosses indicate the time points simulated using the parameter combinations selected by the cutoff criteria (Chi-square + Elbow methods); red crosses indicate those simulated using the nonselected parameter combinations. Gray symbols indicate the clinical data observed in the 3-Dose-RIF study.[7] (c) Violin plots for the directly estimated parameters (β, $CL_{int,all}$, F_aF_g, f_{bile}, $K_{i,u,OATP}$, k_a, and k_{sto}). (d) Violin plots for the transformed parameters ($CL_{int,bile}$, $CL_{int,met}$, $PS_{act,inf}$, $PS_{dif,inf}$, and PS_{eff}). In each plot, a gray area indicates the distribution of the parameter values, a black dot on the violin plot indicates the median, a black bar in the center of the violin indicates interquartile range, solid lines stretched from the bar indicate the 25 percentile and 75 percentile values, and broken lines indicate the lower/upper adjacent values. CGNM, cluster Gauss–Newton method; CL, clearance; PTV, pitavastatin; RIF, rifampicin; SSR, sum of squared residual.

the analysis was too sparse to identify all the parameters in the model. Note that this does not mean that any numerical value of the "unidentifiable" parameters is acceptable to reproduce the blood concentration–time profiles of CP-I under control and RIF-treated conditions. Appropriate parameter combinations of unidentified parameter values are required to exist in the solution space to account for the observed data. The conventional method requires laborious trials to find parameter combinations in the solution space, which can be circumvented by the use of CGNM.

$K_{i,u,OATP}$ could be primarily determined from the peak-to-baseline phase of the CP-I blood concentration with the OATP1B inhibitor.[29] The quartiles for the estimated RIF $K_{i,u,OATP}$ for CP-I (using the reported model for CP-I,[22] and the modified model for RIF) were similar between the analyses of the 2-Dose-RIF and the 3-Dose-RIF

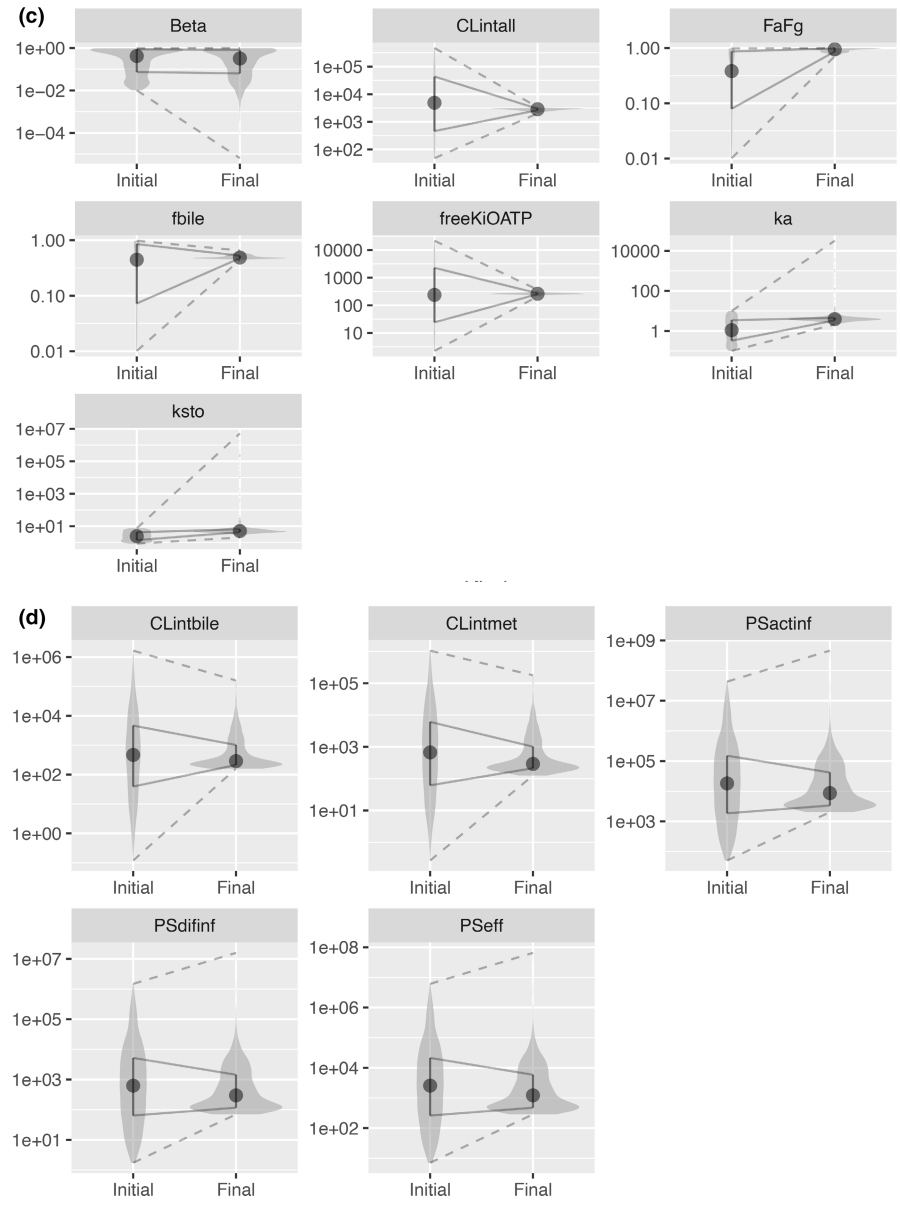

FIGURE 3 (Continued)

studies (0.044–0.055 μM and 0.046–0.060 μM, respectively; Table 1). It is noteworthy that CGNM analysis yielded $K_{i,u,OATP}$ of 0.085 μM when the parameter estimation was carried out under the same conditions as reported previously.[22] We have improved the PBPK model structure for RIF (Figure S1b) to capture its blood concentration–time profiles from the two different clinical studies[7,10] thoroughly during the observation time, which should affect the estimation of $K_{i,u,OATP}$ (Table 1).

We note that the quartiles for $K_{i,u,OATP}$ for PTV and RSV, as the OATP1B probe drugs, obtained by our CGNM analyses (using the reported model for PTV and RSV,[25,26] and the modified model for RIF) were 0.25–0.27 μM and 0.14–0.15 μM, respectively (Table 2), which are within the range of those obtained by our previous analyses for DDIs between statins (PTV and pravastatin) and RIF (0.1–0.3 μM).[26] Hence, the $K_{i,u,OATP}$ values for PTV and RSV obtained in the present study were 4.2–6.1-fold and 2.3–3.4-fold higher, respectively, than those for CP-I (Tables 1 and 2). As far as these individual $K_{i,u,OATP}$ values estimated for CP-I and the OATP1B probe drugs were used, the simulations well explained the observed blood concentration–time profiles (Figures 1b, 2b, 3b, and 4b), AUC, C_{max}, AUCR, and C_{max}R (Figure 5). Therefore, the DDI impact will be inevitably overestimated when $K_{i,u,OATP}$ for CP-I is used in the DDI prediction (statins vs. RIF). Such substrate dependences in $K_{i,u,OATP}$ of RIF have been demonstrated in vitro.[30] Substrate dependence of NCEs on $K_{i,u,OATP}$ can be assessed in the preclinical stages for the translation of CP-I data to DDIs with OATP1B probe substrates, as we emphasized in our previous paper.[22]

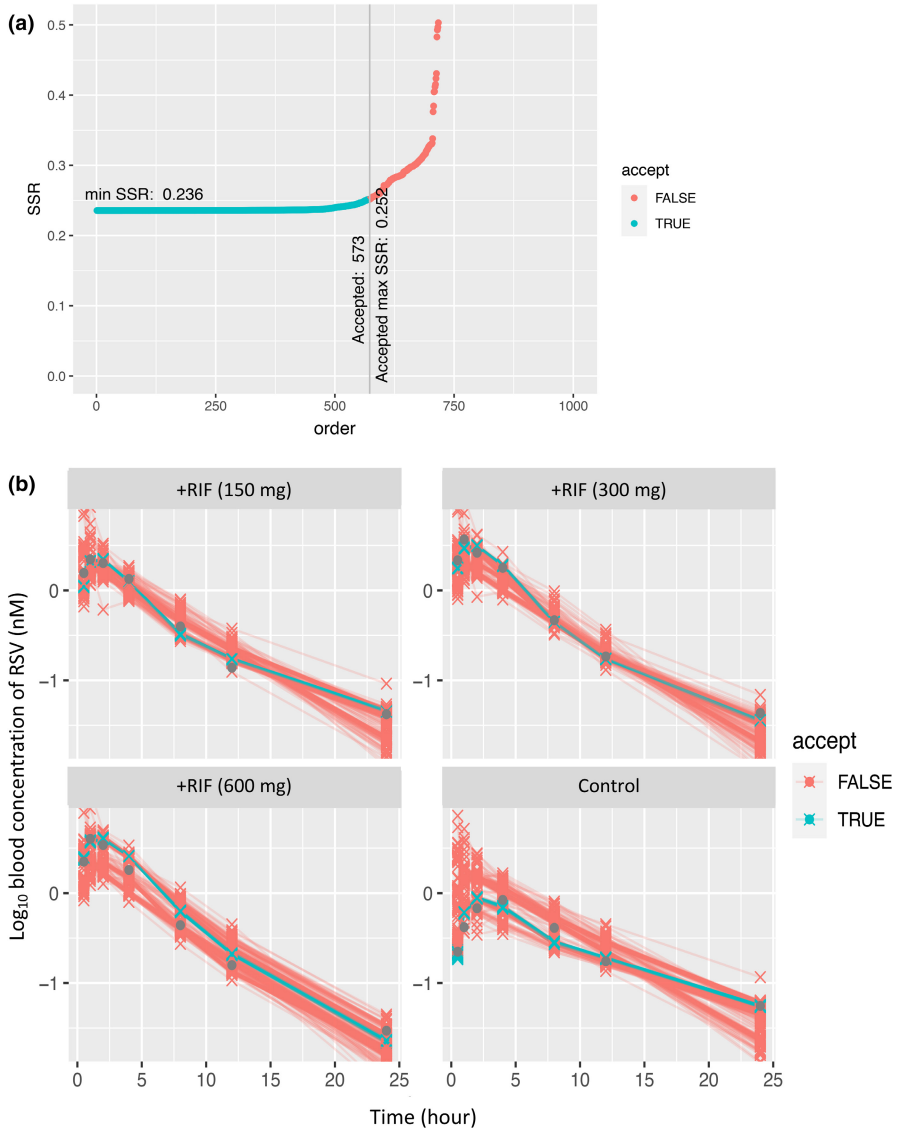

FIGURE 4 Parameter estimation by CGNM using the blood concentration–time profiles of RSV in the 3-Dose-RIF study. (a) The SSR values for 1000 parameter combinations estimated by CGNM analyses are plotted in ascending order. Green dots indicate SSR values less than 0.252 (from ranks 1 to 573) selected by the cutoff criteria (Chi-square + Elbow methods); red dots indicate SSR values more than the cutoff criteria. The minimum SSR (rank 1) was 0.236. (b) The blood concentration–time profiles of RSV in the absence and presence of RIF were simulated using the parameter combinations obtained by CGNM analyses. Green crosses indicate the time points simulated using the parameter combinations selected by the cutoff criteria (Chi-square + Elbow methods); red crosses indicate those simulated using the nonselected parameter combinations. Gray symbols indicate the clinical data observed in the 3-Dose-RIF study.[7] (c) Violin plots for the directly estimated parameters (β, $CL_{int,all}$, F_aF_g, f_{bile}, $K_{i,u,OATP}$, and k_a). (d) Violin plots for the transformed parameters ($CL_{int,bile}$, $CL_{int,met}$, $PS_{act,inf}$, $PS_{dif,inf}$, and PS_{eff}). In each plot, a gray area indicates the distribution of the parameter values, a black dot on the violin plot indicates the median, a black bar in the center of violin indicates interquartile range, solid lines stretched from the bar indicate the 25 percentile and 75 percentile values, and broken lines indicate the lower/upper adjacent values. CGNM, cluster Gauss–Newton method; CL, clearance; RIF, rifampicin; RSV, rosuvastatin; SSR, sum of squared residual.

In our previous analyses,[22] on the basis of a negligible diurnal variation of plasma CP-I, we applied equations that could calculate v_{syn} from $CL_{int,all}$ and steady-state CP-I concentrations calculated on our PBPK model. By fitting using a conventional method (i.e., Gauss–Newton method), the estimated $CL_{int,all}$ was 38 L/h/kg and the calculated v_{syn} was 0.26 nmol/h/kg (with the β value fixed at 0.5) for the 2-Dose-RIF study.[22] This result was reproduced in the present study. First, when applying similar settings (i.e., the same clinical data, the PBPK model structures and fixed parameters for CP-I and RIF, and the number and kind of unknown parameters for CP-I) to the CGNM analyses, the obtained values for $CL_{int,all}$ and v_{syn} were 41 L/h/kg and 0.24 nmol/h/kg, respectively

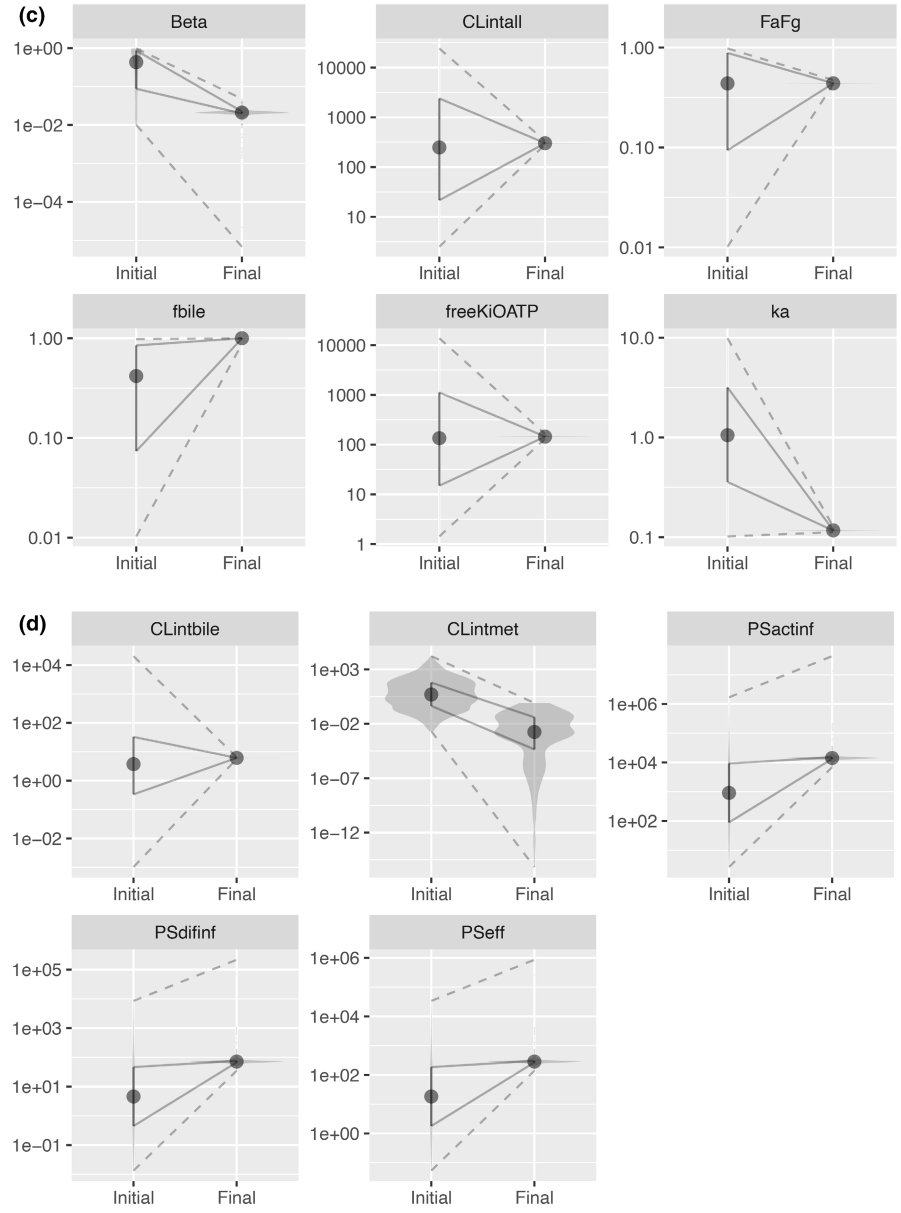

FIGURE 4 (Continued)

(Table S3). Subsequently, when using the improved RIF model and setting more numbers of unknown parameters in CGNM analyses, the quartiles for the estimated $CL_{int,all}$ in the 2-Dose-RIF and the 3-Dose-RIF studies were 41–48 and 35–43 L/h/kg, respectively. The quartiles for the estimated v_{syn} were 0.20–0.25 and 0.17–0.22 nmol/h/kg. Thus, $CL_{int,all}$ and v_{syn} obtained by the CGNM were close to the values obtained by the conventional method, both of which well-reproduce PK of CP-I and DDI effect by RIF as summarized in a table in the Supplementary Text. We found that $CL_{int,all}$ of CP-I could be determined based primarily on the baseline-to-peak phase of its blood concentration through analysis of the clinical data where cyclosporin A, another strong inhibitor for OATP1B, was used as the OATP1B perpetrator.[29] $CL_{int,all}$ in the present study could also be determined from the observed baseline-to-peak phase under the condition that the rate-limiting step (uptake) of hepatic elimination was strongly inhibited by RIF. This subsequently enabled the determination of v_{syn} from the steady-state data without RIF.

In contrast with the convergence of $K_{i,u,OATP}$ by CGNM analyses, it should be impossible to determine $K_{i,u,MRP2}$ using only blood concentration data. The RIF-mediated increase in the blood concentration of CP-I was almost captured when the PBPK model without the RIF-mediated inhibition of hepatic MRP2 was used (data not shown), even though the minimum SSRs (0.0261 and 0.0439 for the 2-Dose-RIF and 3-Dose-RIF studies, respectively) were somewhat larger than those obtained using the model

TABLE 2 Parameters estimated by the CGNM analyses using the blood concentration-time profiles of statins in the 3-Dose-RIF study

Parameter	Unit	Compound name	Minimum	25th percentile	Median	75th percentile	Maximum
β	-	PTV	0.00001	0.0635	0.320	0.813	0.999
		RSV	0.00001	0.0199	0.021	0.023	0.048
$CL_{int,all}$	L/h/kg	PTV	33.9	44.5	48.2	50.4	57.0
		RSV	4.79	5.08	5.09	5.13	5.65
F_aF_g	-	PTV	0.709	0.862	0.947	0.984	1.00
		RSV	0.429	0.438	0.439	0.440	0.474
f_{bile}	-	PTV	0.441	0.475	0.488	0.527	0.653
		RSV	0.874	0.994	1.00	1.00	1.00
$K_{i,u,OATP}$	nmol/L	PTV	208	252	262	274	368
		RSV	131	144	145	146	164
k_a	h^{-1}	PTV	2.13	3.40	3.91	4.57	3.19E+04
		RSV	0.112	0.117	0.117	0.117	0.128
k_{sto}	h^{-1}	PTV	2.04	4.30	5.00	6.49	5.20E+06
		RSV	Not used in the PBPK model				
$PS_{act,inf}$[a]	L/h/kg	PTV	34.2	56.7	146	703	7.75E+06
		RSV	116	225	240	254	7.25E+05
$PS_{dif,inf}$[b]	L/h/kg	PTV	1.18	1.96	5.03	24.2	2.67E+05
		RSV	0.584	1.13	1.21	1.28	3639
PS_{eff}[c]	L/h/kg	PTV	4.84	8.02	20.6	99.4	1.10E+06
		RSV	2.34	4.52	4.82	5.11	1.46E+04
$CL_{int,bile}$[d]	L/h/kg	PTV	2.70	3.58	4.85	17.1	2675
		RSV	0.0949	0.103	0.104	0.104	0.110
$CL_{int,met}$[e]	L/h/kg	PTV	2.11	3.61	4.92	17.1	2995
		RSV	0	6.11E-07	0.0000288	0.000656	0.0138

Note: $CL_{int,all} = (PS_{act,inf} + PS_{dif,inf}) * \beta$; $\beta = (CL_{int,bile} + CL_{int,met})/(PS_{eff} + CL_{int,bile} + CL_{int,met})$; $R_{dif} = PS_{dif,inf}/PS_{act,inf}$; $\gamma = PS_{dif,inf}/PS_{eff}$; $f_{bile} = CL_{int,bile}/(CL_{int,bile} + CL_{int,met})$.[26]

Abbreviations: CGNM, cluster Gauss–Newton method; PBPK, physiologically-based pharmacokinetic; PTV, pitavastatin; RIF, rifampicin; RSV, rosuvastatin.

[a–e]Hepatic intrinsic clearances for membrane permeation and metabolism processes were transformed from the estimated hybrid parameters ($CL_{int,all}$, β and f_{bile}) and the fixed hybrid parameters (R_{dif} = 0.0345 (PTV) or 0.005 (RSV) and γ = 0.244 (PTV) or 0.25 (RSV), as described in Table S1) using the equations as follows:

[a]$PS_{eff} = R_{dif}/(1 + R_{dif})/\gamma * CL_{int,all}/\beta$.

[b]$CL_{int,met} = CL_{int,all}/(1 - \beta) * R_{dif}/(1 + R_{dif})/\gamma * (1 - f_{bile})$.

[c]$PS_{act,inf} = 1/(1 + R_{dif}) * CL_{int,all}/\beta$.

[d]$PS_{dif,inf} = R_{dif}/(1 + R_{dif}) * CL_{int,all}/\beta$.

[e]$CL_{int,bile} = CL_{int,all}/(1 - \beta) * R_{dif}/(1 + R_{dif})/\gamma * f_{bile}$.

These equations are derived from those reported for calculating the hybrid parameters.[26]

incorporating both OATP1B and MRP2 inhibition (0.0259 and 0.0412 for the 2-Dose-RIF and 3-Dose-RIF studies, respectively, as shown in Figures 1 and 2). Taking the in vivo estimation of $K_{i,u,MRP2}$ (0.87 μM)[22] obtained from the PET imaging study into account, the difference between the estimated and observed $K_{i,u,MRP2}$ were also included into the SSR (SSR′, Equation 2). This is a novel approach to loosely constrain the value of $K_{i,u,MRP2}$ in parameter optimization and offers an option to improve the parameter estimation.

The other estimated parameters (β, f_{bile}, F_aF_g, and f_{syn}) of CP-I were not characterized as sensitive, suggesting they have minimal impacts on blood concentration–time profiles in the absence and presence of RIF. CGNM should ensure the feasibility of parameter optimization without fixing these "unidentifiable" parameters. As for f_{syn}, sensitivity analyses of f_{syn} in our previous study demonstrated little effect on the simulated blood concentrations of CP-I with RIF.[22] Similar results were obtained by Takita et al.[23] Their sensitivity analyses showed a marginal impact of the assumption of the CP-I biosynthesis site (blood or liver), resulting in comparable recovery of plasma and urine CP-I data. It might be difficult to determine f_{syn}

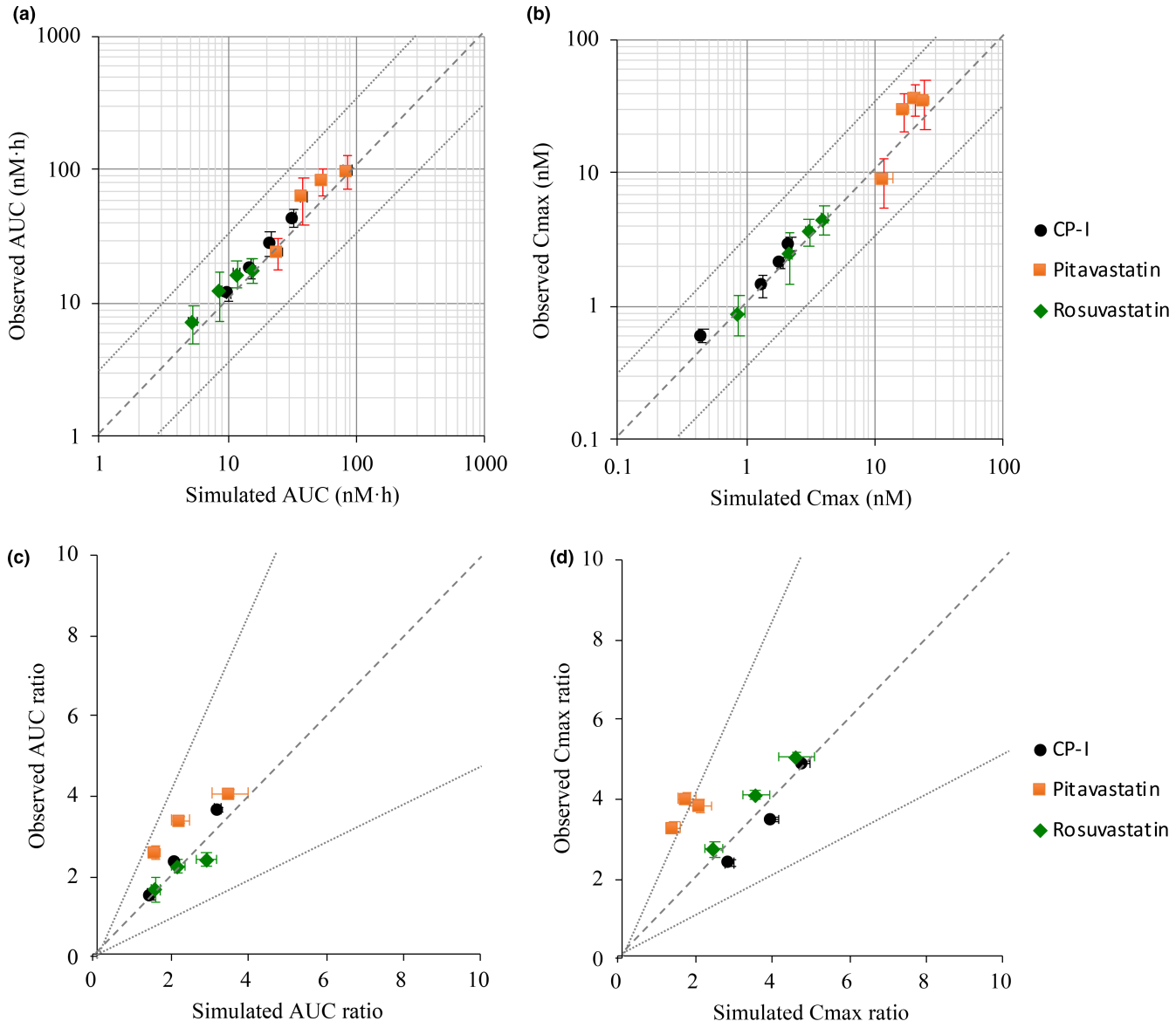

FIGURE 5 Comparison of the observed AUC, C_{max}, AUCR, and C_{max}R with those simulated using the estimated parameter combinations by CGNM. (a and b) The AUC (a) and C_{max} (b) of CP-I, PTV, and RSV in the absence and presence of RIF in the 3-Dose-RIF study[7] are plotted. In each simulation, all the estimated parameter combinations selected by the cutoff method after CGNM analyses were used. Simulated and observed data are presented as mean ± SD. Broken and dotted lines denote unity and three-fold boundaries, respectively. (c and d) The AUCR (c) and C_{max}R (d) of CP-I, PTV, and RSV in the absence and presence of RIF in the 3-Dose-RIF study[7] are plotted. The simulated and observed data are presented as mean ± SD. Broken and dotted lines denote unity and two-fold boundaries, respectively. AUC, area under the blood concentration–time curve; AUCR, area under the blood concentration–time curve ratio; CGNM, cluster Gauss–Newton method; C_{max}, maximum blood concentration; C_{max}R, maximum blood concentration ratio; CP-I, coproporphyrin I; PTV, pitavastatin; RSV, rosuvastatin.

from human data because no matter which organs or tissues are involved in the biosynthesis of CP-I, the effect of RIF-mediated inhibition of OATP1B on the blood concentration–time profile of CP-I should be similar.

In conclusion, CGNM was capable of finding multiple parameter combinations that could capture the CP-I blood concentration data with or without RIF treatment from two different clinical studies. Similar $CL_{int,all}$, $K_{i,u,OATP}$, and v_{syn} values were obtained between the two different clinical studies and as such these parameters were deemed essential for predicting the effect of OATP1B inhibition by RIF. Because it was possible to successfully apply the CGNM to CP-I, we conclude that a similar approach could support the development of PBPK models for additional biomarkers for hepatic OATP1B (e.g., bilirubin and its glucuronides, bile acids, especially glucuronide and sulfate conjugates, glucuronide and sulfate conjugates of steroids, and fatty acid dicarboxylates[5–7]) and for

other transporters, in which their synthesis and clearance mechanisms, diurnal variation, and involvement of other transporters and metabolic enzymes in the observed DDI should be carefully incorporated. In turn, the PBPK model-enabled application of biomarkers in support of clinical DDI risk assessment will greatly facilitate the drug development process, by prioritizing drug probe-based clinical DDI studies only when necessary, by helping to address conservative agency DDI risk thresholds, and by reducing the number of false positive perpetrator compounds being studied clinically.[5,19]

AUTHOR CONTRIBUTIONS

T.Y., Y.A., A.D.R., K.C., H.K., and Y.S. wrote the manuscript. T.Y., Y.A., H.K., and Y.S. designed the research. T.Y., Y.A., T.M., H.K., and Y.S. performed the research. T.Y., Y.A., and Y.S. analyzed the data. T.Y., Y.A., and Y.S. contributed new analytical tools.

FUNDING INFORMATION

This study was financially supported by Grant-in-Aid for Scientific Research (B) (Grant 19H03392) and Grant-in-Aid for Scientific Research (C) (Grant 20K07209) from the Ministry of Education, Culture, Sports, Sciences, and Technology in Japan.

CONFLICT OF INTEREST

The authors declared no competing interests for this work.

ORCID

Koji Chiba https://orcid.org/0000-0001-7600-7813

REFERENCES

1. Morrissey KM, Wen CC, Johns SJ, Zhang L, Huang SM, Giacomini KM. The UCSF-FDA TransPortal: a public drug transporter database. *Clin Pharmacol Ther*. 2012;92(5):545-546.
2. Yoshida K, Maeda K, Sugiyama Y. Transporter-mediated drug--drug interactions involving OATP substrates: predictions based on in vitro inhibition studies. *Clin Pharmacol Ther*. 2012;91(6):1053-1064.
3. Elsby R, Hilgendorf C, Fenner K. Understanding the critical disposition pathways of statins to assess drug-drug interaction risk during drug development: it's not just about OATP1B1. *Clin Pharmacol Ther*. 2012;92(5):584-598.
4. Snoeys J, Beumont M, Monshouwer M, Ouwerkerk-Mahadevan S. Mechanistic understanding of the nonlinear pharmacokinetics and intersubject variability of simeprevir: a PBPK-guided drug development approach. *Clin Pharmacol Ther*. 2016;99(2):224-234.
5. Chu X, Liao M, Shen H, et al. Clinical probes and endogenous biomarkers as substrates for transporter drug-drug interaction evaluation: perspectives from the international transporter consortium. *Clin Pharmacol Ther*. 2018;104(5):836-864.
6. Barnett S, Ogungbenro K, Menochet K, Shen H, Humphreys WG, Galetin A. Comprehensive evaluation of the utility of 20 endogenous molecules as biomarkers of OATP1B inhibition compared with rosuvastatin and coproporphyrin I. *J Pharmacol Exp Ther*. 2019;368(1):125-135.
7. Mori D, Kimoto E, Rago B, et al. Dose-dependent inhibition of OATP1B by rifampicin in healthy volunteers: comprehensive evaluation of candidate biomarkers and OATP1B probe drugs. *Clin Pharmacol Ther*. 2020;107(4):1004-1013.
8. Shen H, Dai J, Liu T, et al. Coproporphyrins I and III as functional markers of OATP1B activity: in vitro and in vivo evaluation in preclinical species. *J Pharmacol Exp Ther*. 2016;357(2):382-393.
9. Lai Y, Mandlekar S, Shen H, et al. Coproporphyrins in plasma and urine can be appropriate clinical biomarkers to recapitulate drug-drug interactions mediated by organic anion transporting polypeptide inhibition. *J Pharmacol Exp Ther*. 2016;358(3):397-404.
10. Takehara I, Yoshikado T, Ishigame K, et al. Comparative study of the dose-dependence of OATP1B inhibition by rifampicin using probe drugs and endogenous substrates in healthy volunteers. *Pharm Res*. 2018;35(7):138.
11. Sane RS, Cheung KWK, Cho E, et al. Evaluation of Ipatasertib interactions with itraconazole and coproporphyrin I and III in a single drug interaction study in healthy subjects. *J Pharmacol Exp Ther*. 2021;378(2):87-95.
12. Feng S, Bo Q, Coleman HA, et al. Further evaluation of coproporphyrins as clinical endogenous markers for OATP1B. *J Clin Pharmacol*. 2021;61(8):1027-1034.
13. Kalluri HV, Kikuchi R, Coppola S, et al. Coproporphyrin I can serve as an endogenous biomarker for OATP1B1 inhibition: assessment using a Glecaprevir/Pibrentasvir clinical study. *Clin Transl Sci*. 2021;14(1):373-381.
14. Jones NS, Yoshida K, Salphati L, Kenny JR, Durk MR, Chinn LW. Complex DDI by Fenebrutinib and the use of transporter endogenous biomarkers to elucidate the mechanism of DDI. *Clin Pharmacol Ther*. 2020;107(1):269-277.
15. Cheung KWK, Yoshida K, Cheeti S, et al. GDC-0810 pharmacokinetics and transporter-mediated drug interaction evaluation with an endogenous biomarker in the first-in-human. *Dose Escalation Study Drug Metab Dispos*. 2019;47(9):966-973.
16. Tsuboya A, Kubota Y, Ishida H, et al. Minimal contribution of the hepatic uptake transporter OATP1B1 to the inter-individual variability in SN-38 pharmacokinetics in cancer patients without severe renal failure. *Cancer Chemother Pharmacol*. 2021;88(3):543-553.
17. Mori D, Ishida H, Mizuno T, et al. Alteration in the plasma concentrations of endogenous organic anion-transporting polypeptide 1B biomarkers in patients with non-small cell lung cancer treated with paclitaxel. *Drug Metab Dispos*. 2020;48(5):387-394.
18. Robbins JA, Menzel K, Lassman M, et al. Acute and chronic effects of rifampin on Letermovir suggest transporter inhibition and induction contribute to Letermovir pharmacokinetics. *Clin Pharmacol Ther*. 2021;111:664-675.
19. Rodrigues AD, Taskar KS, Kusuhara H, Sugiyama Y. Endogenous probes for drug transporters: balancing vision with reality. *Clin Pharmacol Ther*. 2018;103(3):434-448.
20. Barnett S, Ogungbenro K, Menochet K, et al. Gaining mechanistic insight into coproporphyrin I as endogenous biomarker for OATP1B-mediated drug-drug interactions using population pharmacokinetic modeling and simulation. *Clin Pharmacol Ther*. 2017;104:564-574.

21. Yoshida K, Guo C, Sane R. Quantitative prediction of OATP-mediated drug-drug interactions with model-based analysis of endogenous biomarker kinetics. *CPT Pharmacometrics Syst Pharmacol*. 2018;7:517-524.
22. Yoshikado T, Toshimoto K, Maeda K, et al. PBPK modeling of coproporphyrin I as an endogenous biomarker for drug interactions involving inhibition of hepatic OATP1B1 and OATP1B3. *CPT Pharmacometrics Syst Pharmacol*. 2018;7(11):739-747.
23. Takita H, Barnett S, Zhang Y, et al. PBPK model of coproporphyrin I: evaluation of the impact of SLCO1B1 genotype, ethnicity, and sex on its inter-individual variability. *CPT Pharmacometrics Syst Pharmacol*. 2021;10(2):137-147.
24. Aoki Y, Hayami K, Toshimoto K, Sugiyama Y. Cluster gauss–Newton method: an algorithm for finding multiple approximate minimisers of nonlinear least squares problems with applications to parameter estimation of pharmacokinetic models. *Optim Eng*. 2020;23:1-31.
25. Asaumi R, Menzel K, Lee W, et al. Expanded physiologically-based pharmacokinetic model of rifampicin for predicting interactions with drugs and an endogenous biomarker via complex mechanisms including organic anion transporting polypeptide 1B induction. *CPT Pharmacometrics Syst Pharmacol*. 2019;8(11):845-857.
26. Yoshikado T, Yoshida K, Kotani N, et al. Quantitative analyses of hepatic OATP-mediated interactions between statins and inhibitors using PBPK modeling with a parameter optimization method. *Clin Pharmacol Ther*. 2016;100(5):513-523.
27. Futatsugi A, Toshimoto K, Yoshikado T, Sugiyama Y, Kato Y. Evaluation of alteration in hepatic and intestinal BCRP function in vivo from ABCG2 c.421C>a polymorphism based on PBPK analysis of rosuvastatin. *Drug Metab Dispos*. 2018;46(5):749-757.
28. Takashima T, Kitamura S, Wada Y, et al. PET imaging-based evaluation of hepatobiliary transport in humans with (15R)-11C-TIC-me. *J Nucl Med*. 2012;53(5):741-748.
29. Mochizuki T, Aoki Y, Yoshikado T, et al. Physiologically-based pharmacokinetic model-based translation of OATP1B-mediated drug-drug interactions from coproporphyrin I to probe drugs. *Clin Transl Sci*. 2022;15(6):1519-1531.
30. Izumi S, Nozaki Y, Maeda K, et al. Investigation of the impact of substrate selection on in vitro organic anion transporting polypeptide 1B1 inhibition profiles for the prediction of drug-drug interactions. *Drug Metab Dispos*. 2015;43(2):235-247.

SUPPORTING INFORMATION

Additional supporting information can be found online in the Supporting Information section at the end of this article.

How to cite this article: Yoshikado T, Aoki Y, Mochizuki T, et al. Cluster Gauss-Newton method analyses of PBPK model parameter combinations of coproporphyrin-I based on OATP1B-mediated rifampicin interaction studies. *CPT Pharmacometrics Syst Pharmacol*. 2022;11:1341-1357. doi:10.1002/psp4.12849